2022 American Control Conference
Atlanta, USA, June 8-10, 2022

Adaptive Force Control for Small Celestial Body Sampling

Nima Mohseni[1], Dennis S. Bernstein[1], and Marco B. Quadrelli[2]

Abstract— **An adaptive force control algorithm for small celestial body sampling for a variety of surface properties is developed. The control algorithm consists of an adaptive controller combined with feedback linearization. When a spacecraft makes contact with the surface, it must maintain a desired contact force in order to capture a sample. The properties of the surface are unknown or uncertain before contact with the surface is made. The adaptive controller performs system identification online to create an input-output model of the feedback linearized system. From the input-output model a block observable canonical form is realized and the control input is determined by model predictive control (MPC) to maintain a desired contact force in spite of the unknown surface properties. The approach is applied to a variety of surface properties with linear and nonlinear contact models.**

I. Introduction

Surface sampling of small celestial bodies has received increasing interest as seen by recent missions such as OSIRIS-REx, Hayabusa, and Hayabusa2. The objective of a sampling mission is to bring a spacecraft with a sampler in contact with the surface of a celestial body and maintain a desired contact force in order to capture a sample from the surface [1], [2]. The resulting samples are used to further scientific knowledge about the origins of the solar system and universe.

Despite recent successes, surface sampling remains a challenging problem. Before contact with the surface, surface properties such as its compliance are uncertain. Additional challenges arise due to unknown nonlinear contact dynamics, and inability to use the spacecraft thrusters to augment the contact force. Therefore the controller must be designed to be robust to a wide variety of surface properties. If the true surface properties are outside expectations, mission performance will be affected adversely. This was evidenced by the Philae lander which attempted to land on the comet 67P/Churyumov–Gerasimenko and instead bounced off of the surface and landed in the shadow of the comet ending a 10 year long mission early due to the surface being softer than expected [3]. Additionally, there is an inherent trade-off between robustness and control performance which may limit the possible scope of the mission. As sampling missions become increasingly complex, as shown by sampling mission concepts using shape memory alloy and harpoon sampling mechanisms, more advanced control algorithms will be needed [4], [5].

The challenges associated with surface sampling missions motivates an alternative adaptive approach to the surface sampling control problem. The proposed control algorithm consists of a feedback linearization controller along with an adaptive controller called *predictive cost adaptive control* (PCAC) to adaptively regulate the contact force of the sampler when subject to a surface with unknown properties. The following paper proposes an extension of the robust control algorithm given in [6] to the case of an adaptive controller.

PCAC is an adaptive control algorithm developed in [7], [8], which uses a combination of online identification using recursive least squares (RLS) and model predictive control (MPC) to control uncertain or unknown systems. The identification uses an input-output model structure with a variable rate forgetting (VRF) factor to quickly adjust modeling coefficients when new information is received and to prevent adjusting modeling coefficients in the presence of noise. The identified model is then transformed into a block observable canonical form (BOCF) with a known state to be used in MPC without needing an explicit observer.

The structure of the paper is as follows. Section II describes the spacecraft and contact dynamics of a 2D sampling mission. Section III formulates the PCAC algorithm. Section IV describes the combined feedback linearization and PCAC control algorithm, and Section V investigates the performance of the proposed algorithm under various surface properties for both linear and nonlinear contact models.

II. Spacecraft Dynamics and Modeling

An overview of the spacecraft equations of motion and contact dynamics are given in this section. For simplicity, we assume a two-dimensional model, where all masses are rigid. Consider the spacecraft with a 2-link sampling arm as shown in Figure 1. The relative joint angles are given by θ_1 and θ_2, the control torques by τ_1 and τ_2, the spacecraft bus mass by m_{sc}, the link masses and inertias by m_1, m_2, $\bar{I}_1$, and $\bar{I}_2$ respectively, the sampler position relative to the surface by x and y, and the sampler mass by m_s. Contact and friction forces due to the surface are given by F_c and F_f. Due to the small gravitational forces in this environment, gravitational forces are assumed to be negligible relative to the contact forces and are ignored during the contact phase. The resulting equations of motion have the form

$$M(q)\ddot{q} + D(q,\dot{q})\dot{q} = Q \tag{1}$$

$$q \triangleq \begin{bmatrix} \theta_1 \\ \theta_2 \\ x \\ y \end{bmatrix}, \quad \dot{q} \triangleq \begin{bmatrix} \dot{\theta}_1 \\ \dot{\theta}_2 \\ \dot{x} \\ \dot{y} \end{bmatrix}, \tag{2}$$

where $M(q)$, $D(q,\dot{q})$, and Q are the mass, damping and generalized force matrices. Details of the derivation and structure of these matrices are given in [6]. During contact, the generalized

[1]Department of Aerospace Engineering, The University of Michigan, Ann Arbor, MI 48109, USA

[2]Jet Propulsion Laboratory, California Institute of Technology, 4800 Oak Grove Dr., Pasadena, CA 91109, USA

force is given by

$$Q = \begin{bmatrix} 1 & 1 & 0 & 0 \\ 0 & 1 & 0 & 0 \\ 0 & 0 & 1 & 0 \\ 0 & 0 & 0 & 1 \end{bmatrix} \begin{bmatrix} \tau_1 \\ \tau_2 \\ F_\mathrm{f} \\ F_\mathrm{c} \end{bmatrix}. \tag{3}$$

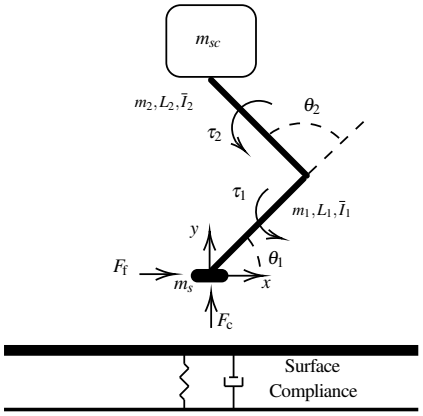

Fig. 1. Spacecraft model for celestial body sampling.

Two forms of the contact force commonly used for contact modeling of small celestial body sampling are now introduced. First, a linear Kelvin-Voigt model [9] with stiffness k_s and damping c_s of the surface material given by

$$F_\mathrm{c} = -k_s y - c_s \dot{y}, \tag{4}$$

and a nonlinear Hunt-Crossley model [10], [11] with coefficient of restitution c_r, stiffness k_s, and initial contact velocity $\dot{y}^-$ given by

$$F_\mathrm{c} = k_s(-y)^{\frac{3}{2}} \left(1 + \frac{3(1-c_r)}{2} \frac{\dot{y}}{\dot{y}^-}\right). \tag{5}$$

Since the contact event occurs with friction, for the friction model, an approximation of the Coulomb force using a regularized friction coefficient is given by

$$F_\mathrm{f} \triangleq \begin{cases} -\mu \left(\frac{\|\dot{x}\|}{10^{-4}}\right) F_\mathrm{c} \operatorname{sgn}(\dot{x}), & \text{if } 0 \le \frac{\|\dot{x}\|}{10^{-4}} \le 1 \\ -\mu F_\mathrm{c} \operatorname{sgn}(\dot{x}), & 1 < \frac{\|\dot{x}\|}{10^{-4}} \end{cases}, \tag{6}$$

where μ is the coefficient of friction [12].

III. Predictive Cost Adaptive Control

PCAC is formulated in [7] and is restated below for convenience of the reader. PCAC combines online identification with a forgetting factor to handle time-varying parameters and model predictive control in two separate steps.

A. Online Identification

Consider the MIMO input-output model

$$\hat{y}_k = -\sum_{i=1}^{\hat{n}} \hat{F}_i y_{k-i} + \sum_{i=1}^{\hat{n}} \hat{G}_i u_{k-i}, \tag{7}$$

where $k \ge 0$ is the time step, $\hat{n} \ge 1$ is the identification data window, $\hat{F}_k \in \mathbb{R}^{p\times p}$ and $\hat{G}_k \in \mathbb{R}^{p\times m}$ are the estimated model coefficients at step k, and $u_k \in \mathbb{R}^{m\times 1}$, $y_k \in \mathbb{R}^{p\times 1}$, and $\hat{y}_k \in \mathbb{R}^{p\times 1}$ are the inputs, outputs and predicted outputs at step k.

To estimate the coefficients $\hat{F}_k$ and $\hat{G}_k$ online, we use recursive least squares (RLS) with variable-rate forgetting [13]. RLS minimizes the cumulative cost

$$J_k(\hat{w}) = \sum_{i=0}^{k} \frac{\rho_i}{\rho_k} z_i^\mathrm{T}(\hat{w}) z_i(\hat{w}) + \frac{1}{\rho_k} (\hat{w} - w_0)^\mathrm{T} P_0^{-1} (\hat{w} - w_0), \tag{8}$$

where $\rho_k \triangleq \prod_{j=0}^{k} \lambda_j^{-1} \in \mathbb{R}$, $\lambda_k \in (0,1]$ is the forgetting factor, $P_0 \in \mathbb{R}^{[\hat{n}p(m+p)]\times[\hat{n}p(m+p)]}$ is positive definite, and $w_0 \in \mathbb{R}^{[\hat{n}p(m+p)]\times 1}$ is the initial estimate of the coefficient vector. The performance variable $z_i(\hat{w}) \in \mathbb{R}^{p\times 1}$ is defined as

$$z_k(\hat{w}) \triangleq y_k + \sum_{i=1}^{\hat{n}} \hat{F}_i y_{k-i} - \sum_{i=1}^{\hat{n}} \hat{G}_i u_{k-i}, \tag{9}$$

where the vector $\hat{w} \in \mathbb{R}^{[\hat{n}p(m+p)]\times 1}$ of coefficients to be estimated is defined by

$$\hat{w} \triangleq \operatorname{vec}\begin{bmatrix} \hat{F}_1 & \cdots & \hat{F}_{\hat{n}} & \hat{G}_1 & \cdots & \hat{G}_{\hat{n}} \end{bmatrix}. \tag{10}$$

Defining the regressor matrix $\phi_k \in \mathbb{R}^{p\times[\hat{n}p(m+p)]}$ by

$$\phi_k \triangleq \begin{bmatrix} -y_{k-1}^\mathrm{T} & \cdots & -y_{k-\hat{n}}^\mathrm{T} & u_{k-1}^\mathrm{T} & \cdots & u_{k-\hat{n}}^\mathrm{T} \end{bmatrix} \otimes I_p, \tag{11}$$

the performance variable can then be written as

$$z_k(\hat{w}) = y_k - \phi_k \hat{w}. \tag{12}$$

The global minimizer $w_{k+1} \triangleq \operatorname{argmin}_{\hat{w}} J_k(\hat{w})$ is computed by RLS as

$$L_k = \lambda_k^{-1} P_k \tag{13}$$

$$P_{k+1} = L_k - L_k \phi_k^\mathrm{T} (I_p + \phi_k L_k \phi_k^\mathrm{T})^{-1} \phi_k L_k \tag{14}$$

$$w_{k+1} = w_k + P_{k+1} \phi_k^\mathrm{T} (y_k - \phi_k \hat{w}), \tag{15}$$

where $w_{k+1} = \operatorname{vec}\begin{bmatrix} \hat{F}_{1,k+1} & \cdots & \hat{F}_{\hat{n},k+1} & \hat{G}_{1,k+1} & \cdots & \hat{G}_{\hat{n},k+1} \end{bmatrix}$.

The variable-rate forgetting (VRF) factor λ_k is developed in [14] and given by

$$\lambda_k = \frac{1}{1 + \eta g(z_{k-\tau_\mathrm{d}}, \ldots, z_k) \mathbf{1}[g(z_{k-\tau_\mathrm{d}}, \ldots, z_k)]} \tag{16}$$

where $\mathbf{1} : \mathbb{R} \to \{0,1\}$ is the unit step function, and

$$g(z_{k-\tau_d}, \ldots, z_k) \triangleq \sqrt{\frac{\tau_\mathrm{n}}{\tau_\mathrm{d}} \frac{\operatorname{tr}\left(\Sigma_{\tau_\mathrm{n}}(z_{k-\tau_\mathrm{n}}, \ldots, z_k) \Sigma_{\tau_\mathrm{d}}(z_{k-\tau_\mathrm{d}}, \ldots, z_k)^{-1}\right)}{c}} - \sqrt{f}, \tag{17}$$

where $\eta > 0$ and $p \le \tau_\mathrm{n} < \tau_\mathrm{d}$ represent numerator and denominator window lengths, respectively. In (17), Σ_{τ_n} and $\Sigma_{\tau_\mathrm{d}} \in \mathbb{R}^{p\times p}$ are the sample variances of the respective window lengths, c is a constant given by

$$a \triangleq \frac{(\tau_\mathrm{n} + \tau_\mathrm{d} - p - 1)(\tau_\mathrm{d} - 1)}{(\tau_\mathrm{d} - p - 3)(\tau_\mathrm{d} - p)}, \; b \triangleq 4 + \frac{(p\tau_\mathrm{n} + 2)}{(a-1)},$$
$$c \triangleq \frac{p\tau_\mathrm{n}(b-2)}{b(\tau_\mathrm{d} - p - 1)}, \tag{18}$$

$f \triangleq F^{-1}_{p\tau_\mathrm{n}, b}(1-\alpha)$ is a thresholding constant, where $F^{-1}_{p\tau_\mathrm{n}, b}(x)$ is the inverse cumulative distribution function of the F-distribution with degrees of freedom $p\tau_\mathrm{n}$ and b, and α is the significance level [15].

For receding-horizon control, the input-output model (7) is written as the block observable canonical form state-space realization

$$x_{1|k} \triangleq \hat{A}_k \hat{x}_k + \hat{B}_k u_k,$$
$$y_k = \hat{C}\hat{x}_k, \tag{19}$$

where $x_{1|k} \in \mathbb{R}^{\hat{n}p}$ is the one-step predicted state, $\hat{x}_k \triangleq \begin{bmatrix}\hat{x}_{1,k}^{\mathrm{T}} & \cdots & \hat{x}_{\hat{n},k}^{\mathrm{T}}\end{bmatrix}^{\mathrm{T}} \in \mathbb{R}^{\hat{n}p}$ is the state estimate, and

$$\hat{x}_{1,k} \triangleq y_k, \tag{20}$$

$$\hat{x}_{i,k} \triangleq -\sum_{j=1}^{\hat{n}-i+1} \hat{F}_{i+j-1,k+1} y_{k-j} + \sum_{j=1}^{\hat{n}-i+1} \hat{G}_{i+j-1,k+1} u_{k-j}, \ i = 2,\ldots,\hat{n} \tag{21}$$

$$\hat{A}_k \triangleq \begin{bmatrix} -\hat{F}_{1,k+1} & I_p & \cdots & \cdots & 0_{p\times p} \\ \vdots & 0_{p\times p} & \ddots & & \vdots \\ \vdots & \vdots & \ddots & \ddots & 0_{p\times p} \\ \vdots & \vdots & & \ddots & I_p \\ -\hat{F}_{\hat{n},k+1} & 0_{p\times p} & \cdots & \cdots & 0_{p\times p} \end{bmatrix}, \tag{22}$$

$$\hat{B}_k \triangleq \begin{bmatrix} \hat{G}_{1,k+1} \\ \hat{G}_{2,k+1} \\ \vdots \\ \hat{G}_{\hat{n},k+1} \end{bmatrix}, \ \hat{C} \triangleq \begin{bmatrix} I_p & 0_{p\times p} & \cdots & 0_{p\times p} \end{bmatrix}, \tag{23}$$

B. Model Predictive Control

The ℓ-step predicted output of (19) for a sequence of ℓ future controls is given by

$$Y_{1|k,l} = \hat{\Gamma}_{k,\ell} x_{1|k} + \hat{T}_{k,\ell} U_{1|k,\ell}, \tag{24}$$

where

$$Y_{1|k,\ell} \triangleq \begin{bmatrix} y_{1|k} \\ \vdots \\ y_{\ell|k} \end{bmatrix} \in \mathbb{R}^{\ell p}, \quad U_{1|k,\ell} \triangleq \begin{bmatrix} u_{1|k} \\ \vdots \\ u_{\ell|k} \end{bmatrix} \in \mathbb{R}^{\ell m}, \tag{25}$$

and $\hat{\Gamma}_{k,\ell} \in \mathbb{R}^{\ell p \times \hat{n}p}$ and $\hat{T}_{k,\ell} \in \mathbb{R}^{\ell p \times \ell m}$ are

$$\hat{\Gamma}_{k,\ell} \triangleq \begin{bmatrix} \hat{C} \\ \hat{C}\hat{A}_k \\ \vdots \\ \hat{C}\hat{A}_k^{\ell-1} \end{bmatrix}, \tag{26}$$

$$\hat{T}_{k,\ell} \triangleq \begin{bmatrix} 0_{p\times m} & \cdots & \cdots & \cdots & 0_{p\times m} \\ \hat{H}_{k,1} & 0_{p\times m} & \cdots & \cdots & 0_{p\times m} \\ \hat{H}_{k,2} & \hat{H}_{k,1} & \ddots & \cdots & 0_{p\times m} \\ \vdots & \vdots & \ddots & \ddots & \vdots \\ \hat{H}_{k,\ell-1} & \hat{H}_{k,\ell-2} & \cdots & \hat{H}_{k,1} & 0_{p\times m} \end{bmatrix}, \tag{27}$$

where $\hat{H}_{k,i} \in \mathbb{R}^{p\times m}$ is defined by $\hat{H}_{k,i} \triangleq \hat{C}\hat{A}_k^{i-1}\hat{B}_k$.

Let $\mathcal{R}_{k,\ell} \triangleq \begin{bmatrix} r_{k+1}^{\mathrm{T}} \cdots r_{k+\ell}^{\mathrm{T}} \end{bmatrix}^{\mathrm{T}} \in \mathbb{R}^{\ell p_{\mathrm{t}}}$ be the vector of ℓ future commands, $C_{\mathrm{t},\ell} \triangleq I_\ell \otimes C_{\mathrm{t}} \in \mathbb{R}^{\ell p_{\mathrm{t}} \times \ell p}$ where $C_{\mathrm{t}} y_{i|k}$ creates the tracking outputs from $y_{i|k}$, let $Y_{\mathrm{t},1|k,\ell} \triangleq C_{\mathrm{t},\ell} Y_{1|k,\ell}$ be the ℓ-step predicted tracking output, and define $\Delta U_{1|k,\ell} \in \mathbb{R}^{\ell m \times 1}$ as

$$\Delta U_{1|k,\ell} \triangleq \begin{bmatrix} (u_{1|k} - u_k)^{\mathrm{T}} & \cdots & (u_{\ell|k} - u_{\ell-1|k})^{\mathrm{T}} \end{bmatrix}^{\mathrm{T}}. \tag{28}$$

The receding horizon optimization problem is then given by

$$\min_{U_{1|k,\ell}} \left(Y_{\mathrm{t},1|k,\ell} - \mathcal{R}_{k,\ell}\right)^{\mathrm{T}} Q \left(Y_{\mathrm{t},1|k,\ell} - \mathcal{R}_{k,\ell}\right) + \Delta U_{1|k,\ell}^{\mathrm{T}} R \Delta U_{1|k,\ell} \tag{29}$$

subject to

$$U_{\min} \le U_{1|k,\ell} \le U_{\max} \tag{30}$$

$$\Delta U_{\min} \le \Delta U_{1|k,\ell} \le \Delta U_{\max}, \tag{31}$$

where $Q \in \mathbb{R}^{\ell p_{\mathrm{t}} \times \ell p_{\mathrm{t}}}$ is the positive definite tracking weight, $R \in \mathbb{R}^{\ell m \times \ell m}$ is the positive definite control move-size weight, $U_{\min} \triangleq 1_{\ell\times 1} \otimes u_{\min} \in \mathbb{R}^{\ell m}$, $U_{\max} \triangleq 1_{\ell\times 1} \otimes u_{\max} \in \mathbb{R}^{\ell m}$, $\Delta U_{\min} \triangleq 1_{\ell\times 1} \otimes \Delta u_{\min} \in \mathbb{R}^{\ell m}$, and $\Delta U_{\max} \triangleq 1_{\ell\times 1} \otimes \Delta u_{\max} \in \mathbb{R}^{\ell m}$.

IV. Control Algorithm

Following the dynamics derivation given in [6], the mass and damping matrices can be decomposed into the following 2×2 partitions

$$M(q) = \begin{bmatrix} M_1(\overline{\theta}) & M_2(\overline{\theta}) \\ M_2^{\mathrm{T}}(\overline{\theta}) & m_0 I_2 \end{bmatrix},$$
$$D(q,\dot{q}) = \begin{bmatrix} D_1(\overline{\theta},\dot{q}) & D_2(\overline{\theta},\dot{q}) \\ D_2^{\mathrm{T}}(\overline{\theta},\dot{q}) & 0_2 \end{bmatrix}, \ \overline{\theta} \triangleq \begin{bmatrix} \theta_1 \\ \theta_2 \end{bmatrix}, \tag{32}$$

where $m_0 \triangleq m_{sc} + m_1 + m_2 + m_s$. Since θ_1, $\dot{\theta}_1$, θ_2, $\dot{\theta}_2$, $\dot{x}$, $\dot{y}$, and F_{c} are measured, the following feedback linearization controller can be used

$$\begin{bmatrix} \tau_1 \\ \tau_2 \end{bmatrix} = L^{-1}[D_1(\overline{\theta},\dot{q}) \begin{bmatrix} \dot{\theta}_1 \\ \dot{\theta}_2 \end{bmatrix} + D_2(\overline{\theta},\dot{q}) \begin{bmatrix} \dot{x} \\ \dot{y} \end{bmatrix} + M_1(\overline{\theta}) M_2^{-\mathrm{T}}(\overline{\theta}) (-D_2^{\mathrm{T}}(\overline{\theta},\dot{q}) \begin{bmatrix} \dot{\theta}_1 \\ \dot{\theta}_2 \end{bmatrix} + \begin{bmatrix} 0 \\ 1 \end{bmatrix} F_{\mathrm{c}}) + (M_2(\overline{\theta}) - M_1(\overline{\theta}) M_2^{-\mathrm{T}}(\overline{\theta}) m_0 I_2) \begin{bmatrix} \tau_{f,1} \\ \tau_{f,2} \end{bmatrix}], \tag{33}$$

where $\tau_{f,1}$ and $\tau_{f,2}$ are the feedforward portion of the feedback linearization controller to be given by PCAC and $L \triangleq \begin{bmatrix} 1 & 1 \\ 0 & 1 \end{bmatrix}$. For the feedback linearization controller, we assume that the contact force is of the linear form given by (4). Substituting (33) into (1) and taking the derivative of (4) leads to the following dynamics in state-space form

$$\begin{bmatrix} \ddot{\theta}_1 \\ \ddot{\theta}_2 \\ \ddot{x} \\ \ddot{y} \\ \dot{F}_c \end{bmatrix} = A(\overline{\theta},\dot{q}) \begin{bmatrix} \dot{\theta}_1 \\ \dot{\theta}_2 \\ \dot{x} \\ \dot{y} \\ F_{\mathrm{c}} \end{bmatrix} + B(\overline{\theta}) \begin{bmatrix} \tau_{f,1} \\ \tau_{f,2} \end{bmatrix} + E(\overline{\theta}) F_{\mathrm{f}}, \tag{34}$$

$$A(\overline{\theta},\dot{q}) \triangleq \begin{bmatrix} -M_2^{-\mathrm{T}}(\overline{\theta}) D_2^{\mathrm{T}}(\overline{\theta},\dot{q}) & 0 & 0 & M_2^{-\mathrm{T}}(\overline{\theta}) \begin{bmatrix} 0 \\ 1 \end{bmatrix} \\ 0 \ \ 0 & 0 & 0 & 0 \\ 0 \ \ 0 & 0 & 0 & 0 \\ 0 \ \ 0 & 0 & -k_s & 0 \end{bmatrix}, \tag{35}$$

$$B(\overline{\theta}) \triangleq \begin{bmatrix} M_2^{-\mathrm{T}}(\overline{\theta}) m_0 I_2 \\ 1 \quad 0 \\ 0 \quad 1 \\ 0 \quad -c_s \end{bmatrix}, E(\overline{\theta}) \triangleq \begin{bmatrix} M_2^{-\mathrm{T}}(\overline{\theta}) \begin{bmatrix} 1 \\ 0 \end{bmatrix} \\ \xi(\overline{\theta}) \begin{bmatrix} 1 \\ 0 \end{bmatrix} \\ -c_s \begin{bmatrix} 0 & 1 \end{bmatrix} \xi(\overline{\theta}) \begin{bmatrix} 1 \\ 0 \end{bmatrix} \end{bmatrix}, \tag{36}$$

$$\xi(\overline{\theta}) \triangleq \left(M_2(\overline{\theta}) - M_1(\overline{\theta}) M_2^{-\mathrm{T}}(\overline{\theta}) m_0 I_2\right)^{-1} M_1(\overline{\theta}) M_2^{-\mathrm{T}}(\overline{\theta}). \tag{37}$$

If the surface compliance is linear and known, then when using the control architecture shown in Figure 2, the dynamics (34) are what PCAC will attempt to regulate. The frictional force appears as a disturbance through the matrix $E(\overline{\theta})$. In case of a mismatch between the true surface compliance parameters or dynamics, and the parameters used for the feedback linearization control, then (34) is no longer valid and PCAC must attempt to identify online a new model to regulate the closed-loop system.

V. Simulation Examples

Four examples are chosen to demonstrate the performance of the control architecture with regards to a wide variety of surface parameters and available modeling information. In these examples, the spacecraft in Figure 1 descends onto the surface at a speed of $0.1\,\frac{\mathrm{m}}{\mathrm{s}}$ starting from a height of 0.2 m. There are seven sensors measuring θ_1, $\dot{\theta}_1$, θ_2, $\dot{\theta}_2$, $\dot{x}$, $\dot{y}$, and F_{c}. Once contact is made, the controller attempts to regulate the sampler's contact force to 25 N and its x and y velocity to 0 before departing the surface after 2 s.

Sections V-A and V-B assume the surface has the linear Kelvin-Voigt contact model given by (4) while sections V-C and V-D assume the surface has the nonlinear Hunt-Crossley model given by (5). For sections V-A and V-C, the PCAC model coefficients are initialized with w_0 such that the block observable canonical form is similar to the matrices $A(\overline{\theta}, \dot{q})$ and $B(\overline{\theta})$ at $t = 0$. In sections V-B and V-D, PCAC is initialized with the uninformative model where all entries are 10^{-10}. In all cases, the true surface compliance is unknown and for the cases where PCAC is initialized with a model, the initial model matrices assume the surface contact model is linear with $k_s = 100\,\frac{\mathrm{N}}{\mathrm{m}}$ and $c_s = 10^4\,\frac{\mathrm{Ns}}{\mathrm{m}}$. The controller runs in a sample-data feedback loop at 2 kHz.

The spacecraft parameters are $m_{sc} = 420\,\mathrm{kg}$, $m_1 = m_2 = m_s = 1\,\mathrm{kg}$, $L_1 = L_2 = 2\,\mathrm{m}$, $\bar{I}_1 = \bar{I}_2 = \frac{1}{3}\,\frac{\mathrm{kg}}{\mathrm{m}^2}$, $\theta_{1,0} = 45°$, and $\theta_{2,0} = 90°$. The surface coefficient of friction is taken to be $\mu = 0.5$. PCAC is initialized with $p = 5$, $m = 2$, $\hat{n} = 1$, $P_0 = 10 I_{45}$, $\eta = 0.1$, $\tau_{\mathrm{n}} = 40$, $\tau_{\mathrm{d}} = 200$, $\alpha = 0.001$, $\ell = 50$, $Q = I_\ell \otimes \mathrm{diag}(1000, 100, 1)$, $R = 1 I_{\ell m}$, $C_{\mathrm{t}} = \begin{bmatrix} 0_{3\times 2} & I_3 \end{bmatrix}$, $u_{\max} = -u_{\min} = 100$, and $\mathcal{R}_{k,\ell} = 1_{3\times\ell} \otimes \begin{bmatrix} 0 & 0 & 25 \end{bmatrix}^{\mathrm{T}}$.

A. Linear Contact Model With Dynamics Knowledge

Consider a surface with the linear Kelvin-Voigt contact model and PCAC initialized with an initial model as described above. Figure 3 shows the median contact force during contact for a range of stiffness k_s and damping c_s values between $1 - 10^7\,\frac{\mathrm{N}}{\mathrm{m}}$ and $10^{-2} - 10^4\,\frac{\mathrm{Ns}}{\mathrm{m}}$. Notice that the 25 N contact force is maintained over a wide range of values. Lower stiffness prevents the spacecraft from reaching the desired contact force, and high stiffness leads to limitations due to the sample rate. The response for $k_s = 2 \times 10^4\,\frac{\mathrm{N}}{\mathrm{m}}$ and $c_s = 10^3\,\frac{\mathrm{Ns}}{\mathrm{m}}$ is shown in Figure 4.

B. Linear Contact Model Without Dynamics Knowledge

Consider a surface with the linear Kelvin-Voigt contact model and PCAC initialized with the uninformative model $w_0 = 10^{-10} 1_{45\times 1}$. Figure 5 shows the median contact force during contact for a range of stiffness k_s and damping c_s values between $1 - 10^7\,\frac{\mathrm{N}}{\mathrm{m}}$ and $10^{-2} - 10^4\,\frac{\mathrm{Ns}}{\mathrm{m}}$. Despite the lack of modeling knowledge, PCAC was able to adapt and maintain the contact force for a wide range of values. Similarly to the case where PCAC is initialized with an initial model, there are limitations at maintaining the contact force at low and high stiffness values. There are more regions, especially for high stiffness values, where the controller is unable to maintain the desired contact force. The response for $k_s = 2 \times 10^4\,\frac{\mathrm{N}}{\mathrm{m}}$ and $c_s = 10^3\,\frac{\mathrm{Ns}}{\mathrm{m}}$ is shown in Figure 6.

C. Nonlinear Contact Model With Dynamics Knowledge

Consider a surface with the nonlinear Hunt-Crossley contact model and PCAC initialized with an initial model as described above. Figure 7 shows the median contact force during contact for a range of stiffness k_s and coefficient of restitution c_r values between $1 - 10^7\,\frac{\mathrm{N}}{\mathrm{m}}$ and $10^{-1} - 1$. Despite PCAC being initialized assuming linear contact force, the desired contact force is maintained over a wide range of values as PCAC was able to adapt to the model mismatch. Lower stiffness prevents the spacecraft from reaching the desired contact force, and high stiffness leads to limitations due to the sample rate. Empty data points represent values where the controller became unstable. The nonlinear contact model provides less contact force for small surface displacement than the linear model. This leads to a larger region where the desired contact force is not reached for small stiffness values compared to the linear model case. The response for $k_s = 2 \times 10^4\,\frac{\mathrm{N}}{\mathrm{m}}$ and $c_r = 0.95$ is shown in Figure 8.

D. Nonlinear Contact Model Without Dynamics Knowledge

Consider a surface with the nonlinear Hunt-Crossley contact model and PCAC initialized with the uninformative model $w_0 = 10^{-10} 1_{45\times 1}$. Figure 9 shows the median contact force during contact for a range of stiffness k_s and coefficient of restitution c_r values between $1 - 10^7\,\frac{\mathrm{N}}{\mathrm{m}}$ and $10^{-1} - 1$. Similarly to the previous cases, lower stiffness prevents the spacecraft from reaching the desired contact force, and high stiffness leads to limitations due to the sample rate. Empty data points represent values where the controller became unstable. There are more regions, especially at high stiffness values, where the controller becomes unstable or unable to maintain the 25 N contact force than in the case where PCAC is given linear contact dynamics knowledge. The response for $k_s = 2 \times 10^4\,\frac{\mathrm{N}}{\mathrm{m}}$ and $c_r = 0.95$ is shown in Figure 10.

VI. Conclusion

This paper developed and investigated the performance of an adaptive force control algorithm for spacecraft sampling maneuvers on small celestial bodies. The algorithm consisted of feedback linearization with PCAC to maintain a desired contact force during the sampling maneuver. PCAC uses output-feedback model predictive control without an estimator and with concurrent online identification. Both linear and nonlinear contact models were used to investigate the controller's performance under various surface properties and initial modeling information. The controller

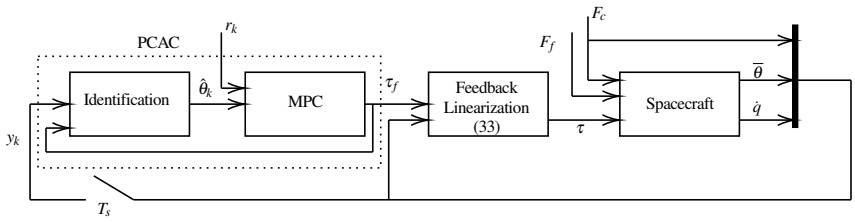

Fig. 2. Adaptive force control architecture for small celestial body sampling.

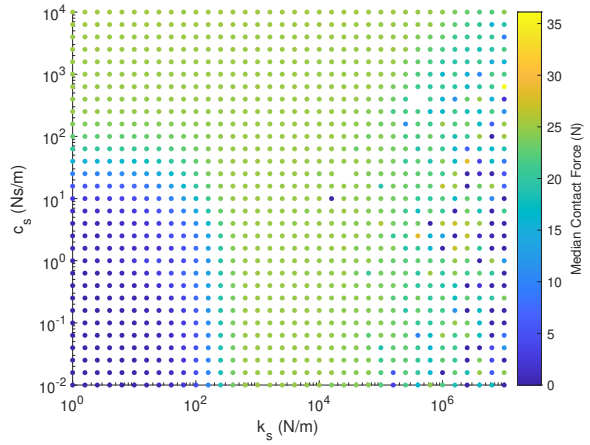

Fig. 3. Median contact force for various surface stiffness k_s and damping c_s values using a linear contact model and PCAC being initialized with modeling information.

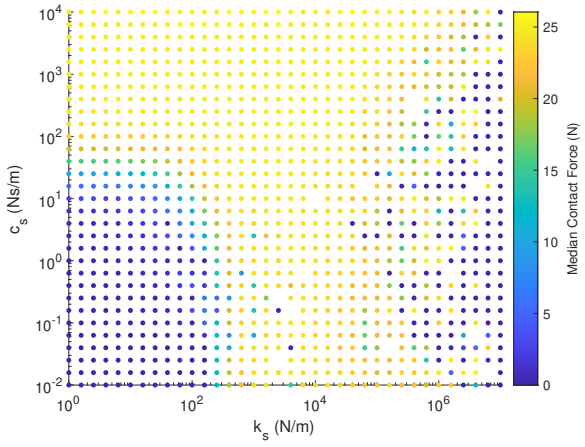

Fig. 5. Median contact force for various surface stiffness k_s and damping c_s values using a linear contact model and PCAC being initialized with an uninformative model.

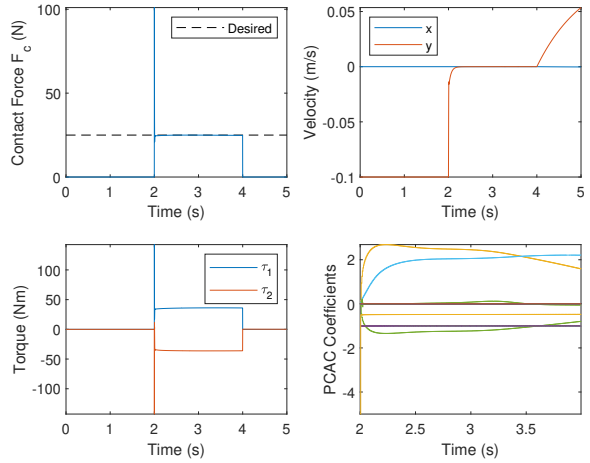

Fig. 4. Contact force, sampler velocity, actuator torques, and PCAC model coefficients for a linear contact model with $k_s = 2 \times 10^4 \frac{\text{N}}{\text{m}}$ and $c_s = 10^3 \frac{\text{Ns}}{\text{m}}$ using PCAC initialized with an initial model.

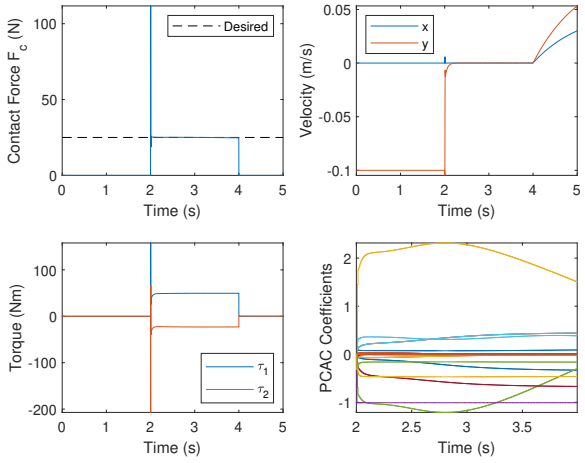

Fig. 6. Contact force, sampler velocity, actuator torques, and PCAC model coefficients for a linear contact model with $k_s = 2 \times 10^4 \frac{\text{N}}{\text{m}}$ and $c_s = 10^3 \frac{\text{Ns}}{\text{m}}$ using PCAC initialized with an uninformative model.

was shown to reach the desired contact force over a wide range of surface properties and initial modeling information for PCAC.

When contact is first made with the surface, there is an initial large transient force exerted on the sampler. This may be mitigated using a combination of the proposed control algorithm and a robust controller. The inclusion of the robust controller will lessen the degree of adaptation required by the adaptive controller and thereby increasing the range of parameters where the desired contact force can be maintained. Further investigation will be needed to determine the advantages of the combined control approach. Additionally, the performance of the control law under multiple sampling maneuvers is of interest. As the sampler increases in mass as more material collected with each maneuver, PCAC can adjust its model accordingly to maintain the desired contact force.

Acknowledgements

This work was supported by a NASA Space Technology Graduate Research Opportunity under grant number 80NSSC20K1164. Government sponsorship acknowledged. This research was carried out at the Jet Propulsion Laboratory,

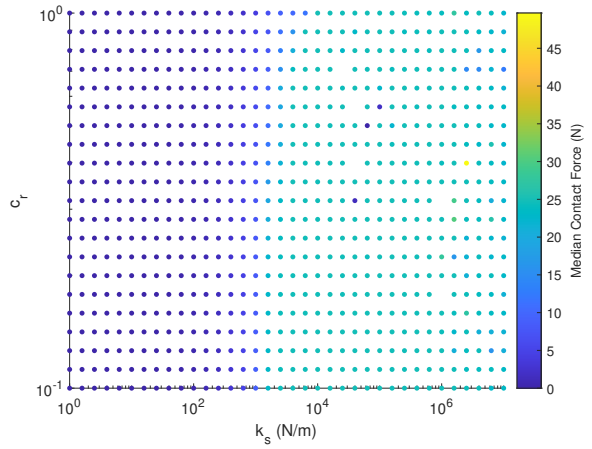

Fig. 7. Median contact force for various surface stiffness k_s and coefficient of restitution c_r values using a nonlinear contact model and PCAC being initialized with modeling information.

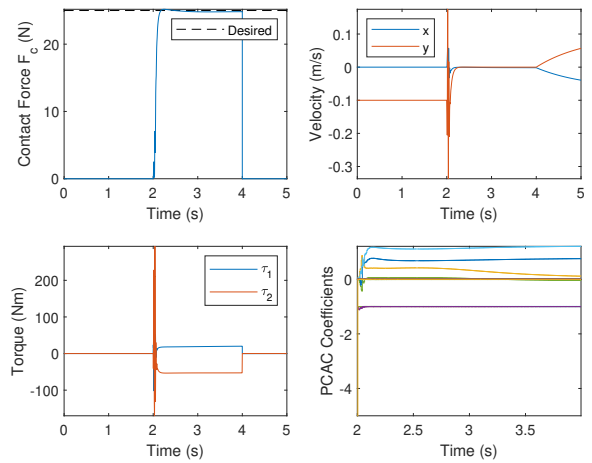

Fig. 8. Contact force, sampler velocity, actuator torques, and PCAC model coefficients for a nonlinear contact model with $k_s = 2 \times 10^4 \frac{\text{N}}{\text{m}}$ and $c_r = 0.95$ using PCAC initialized with an initial model.

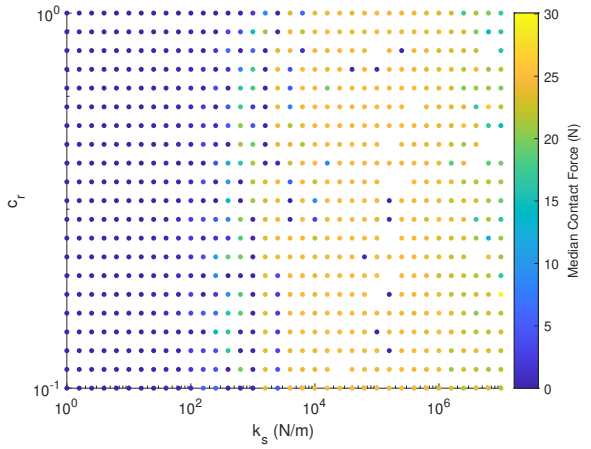

Fig. 9. Median contact force for various surface stiffness k_s and coefficient of restitution c_r values using a nonlinear contact model and PCAC being initialized with an uninformative model.

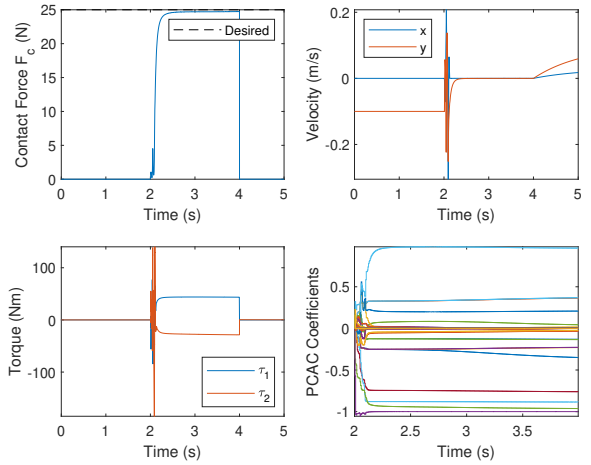

Fig. 10. Contact force, sampler velocity, actuator torques, and PCAC model coefficients for a nonlinear contact model with $k_s = 2 \times 10^4 \frac{\text{N}}{\text{m}}$ and $c_r = 0.95$ using PCAC initialized with an uninformative model. Note that despite the lack of an initial model, the 25 N contact force is maintained soon after contact.

California Institute of Technology, during the first author's summer internship under Dr. Quadrelli's mentorship, under a contract with the National Aeronautics and Space Administration.

References

[1] A. May, B. Sutter, T. Linn, B. Bierhaus, K. Berry, and R. Mink, "Osiris-rex touch-and-go (tag) mission design for asteroid sample collection," *Int. Astronaut. Congr.*, vol. 65, pp. 1–11, 2014.

[2] T. Ajluni, D. Everett, T. Linn, R. Mink, W. Willcockson, and J. Wood, "Osiris-rex, returning the asteroid sample," in *IEEE Aerosp. Conf.*, 2015, pp. 1–15.

[3] J. Biele, S. Ulamec, M. Maibaum, R. Roll, and et al., "The landing(s) of philae and inferences about comet surface mechanical properties," *Science*, vol. 349, no. 6247, pp. 1–6, 2015.

[4] M. B. Quadrelli *et al.*, "Investigation of phase transition-based tethered systems for small body sample capture," *Acta Astronaut.*, vol. 68, no. 7, pp. 947–973, 2011.

[5] M. B. Quadrelli, M. Ono, and A. Jain, "Modeling of active tether system concepts for planetary exploration," *Acta Astronaut.*, vol. 138, pp. 512–529, 2017.

[6] B. Acikmese, M. Quadrelli, and L. Phan, "A force control algorithm for small celestial body surface sampling," *AIAA Guid. Nav. Contr. Conf.*, pp. 1–15, 2007.

[7] T. Nguyen, S. A. U. Islam, D. S. Bernstein, and I. Kolmanovsky, "Predictive cost adaptive control: A numerical investigation of persistency, consistency, and exigency," *IEEE Control Systems Magazine*, 2021.

[8] N. Mohseni, T. W. Nguyen, S. A. Ul Islam, I. V. Kolmanovsky, and D. S. Bernstein, "Active noise control for harmonic and broadband disturbances using rls-based model predictive control," in *Am. Control Conf.*, 2020, pp. 1393–1398.

[9] P. Flores, "Compliant contact force approach for forward dynamic modeling and analysis of biomechanical systems," *Procedia IUTAM*, vol. 2, pp. 58–67, 2011.

[10] K. H. Hunt and F. R. E. Crossley, "Coefficient of Restitution Interpreted as Damping in Vibroimpact," *Journal of Applied Mechanics*, vol. 42, no. 2, pp. 440–445, 1975.

[11] S. R. Schwartz, P. Michel, D. C. Richardson, and H. Yano, "Low-speed impact simulations into regolith in support of asteroid sampling mechanism design i: Comparison with 1-g experiments," *Planetary and Space Science*, vol. 103, pp. 174–183, 2014.

[12] A. M. Castro, A. Qu, N. Kuppuswamy, A. Alspach, and M. Sherman, "A transition-aware method for the simulation of compliant contact with regularized friction," *IEEE Robot. Autom. Lett.*, vol. 5, no. 2, pp. 1859–1866, 2020.

[13] A. L. Bruce, A. Goel, and D. S. Bernstein, "Convergence and consistency of recursive least squares with variable-rate forgetting," *Automatica*, vol. 119, p. 109052, 2020.

[14] N. Mohseni and D. S. Bernstein, "Recursive least squares with variable-rate forgetting based on the f-test," in *Am. Control Conf.*, 2022.

[15] J. J. McKeon, "F approximations to the distribution of Hotelling's T_0^2," *Biometrika*, vol. 61, no. 2, pp. 381–383, 08 1974.